Terbium Fluorescence as a Sensitive, Inexpensive Probe for UV-induced Damage in Nucleic Acids

Amira F. El-Yazbi and Glen R. Loppnow*

Department of Chemistry, University of Alberta, Edmonton, AB T6G 2G2, Canada

*Corresponding author. Tel.: (780) 492-9704; Fax: (780) 492-8231.

E-mail address: glen.loppnow@ualberta.ca (G. R. Loppnow).

Abstract

Much effort has been focused on developing methods for detecting damaged nucleic acids. However, almost all of the proposed methods consist of multi-step procedures, are limited, require expensive instruments, or suffer from a high level of interferences. In this paper, we present a novel simple, inexpensive, mix-and-read assay that is generally applicable to nucleic acid damage and uses the enhanced luminescence due to energy transfer from nucleic acids to terbium(III) (Tb^{3+}). Single-stranded oligonucleotides greatly enhance the Tb^{3+} emission, but duplex DNA does not. With the use of a DNA hairpin probe complementary to the oligonucleotide of interest, the Tb^{3+}/hairpin probe is applied to detect ultraviolet (UV)-induced DNA damage. The hairpin probe hybridizes only with the undamaged DNA. However, the damaged DNA remains single-stranded and enhances the intrinsic fluorescence of Tb^{3+}, producing a detectable signal directly proportional to the amount of DNA damage. This allows the Tb^{3+}/hairpin probe to be used for sensitive quantification of UV-induced DNA damage. The Tb^{3+}/hairpin probe showed superior selectivity to DNA damage compared to conventional molecular beacons probes (MBs) and its sensitivity is more than 2.5 times higher than MBs with

a limit of detection of 4.36 ± 1.2 nM. In addition, this probe is easier to synthesize and more than eight times cheaper than MBs which makes its use recommended for high-throughput, quantitative analysis of DNA damage.

Keywords

Terbium, Fluorescence, Nucleic Acid damage, Hairpin probe, Fluorescence sensor.

1. Introduction

Exposure of nucleic acids to solar UV radiation gives rise to a wide range of photochemical products such as cyclobutane pyrimidine dimers (CPDs), [6-4] pyrimidine-pyrimidinones, dewar pyrimidinone photoproducts and uracil and thymine photohydrates [1,2]. On the other hand, free radicals, such as reactive oxygen species, leads to oxidation products, such as 8-oxoguanosine and photohydrates. Other damage agents, such as reactive chemicals and ionizing radiation, lead to other DNA lesions, such as single- and double-strand breaks, adducts, and cross-links. All these damage products lead to miscoding during DNA replication and may result in mutagenesis, carcinogenesis and cell death [3-6].

Fluorescent methods have been shown to be superior for detecting DNA damage over previous destructive, time-consuming techniques such as gel electrophoresis [7], capillary electrophoresis [8,9], electrochemical [9,10], HPLC [11], mass spectrometric [12-14] and polymerase chain reaction (PCR) amplification [15] methods. Fluorescent probes offer enhanced sensitivity and the potential for use *in situ* or *in vivo*. Differences in the fluorescence lifetime of a dye intercalated in undamaged and damaged DNA have also been used to detect DNA damage [16]. Fluorescently-labeled antibodies provide a highly selective probe of particular damage photoproducts, such as thymine cyclobutyl photodimers [17].

The use of fluorescent nucleic acid probes, such as molecular beacons (MBs) and smart probes, have become powerful tools for application in detection of nucleic acid targets in general [18,19,20], and broad-spectrum detection of different types of DNA and RNA damage such as radiation, oxidative and chemical damage [2,21-24]. For the design of such a probe, the recognition capabilities of DNA through hybridization reactions are well-established, but adequate reporters are needed to generate a physically measurable signal from the hybridization event. This is normally accomplished by labeling the same DNA probe with a fluorophore-quencher pair so that the Förster resonance energy transfer (FRET) can take place. Despite the wide applications and the exquisite sensitivity and selectivity of MBs, they have some readily-apparent limitations [25-30], such as the synthetic and purification difficulties, and limitations associated with site-specific labeling of each terminus of the hairpin [25,26,28,30], incomplete attachment of the quencher [3,7], and its ability to probe only undamaged DNA [2,21-24]. For this last limitation, the MB signal is inversely proportional to the damage, or negative detection, lowering the sensitivity and selectivity of the assay.

The main focus of this work is to design an inexpensive probe for the positive detection of DNA damage, in which the produced signal is directly proportional to the amount of DNA damage. We have previously reported two methods for the positive detection of DNA damage. The first is by using a 2-aminopurine (2AP) hairpin probe [31]. This probe offers high sensitivity and selectivity for the detection of DNA damage, as well as overcoming most of the MB probe's limitations. However, these are expensive probes, especially with an increasing number of 2AP bases incorporated in the probe to increase sensitivity. A hypochromism probe [32] was also designed. The hypochromic effect arises from the formation of the double-stranded hybrid of the undamaged target and hairpin. With accumulated UV exposure, the target-hairpin hybrid

concentration decreases and the absorbance increases. This probe is more selective and is more than ten times cheaper than MBs, but is less sensitive [32]. The goal of this paper is to design a more sensitive, selective and cheaper probe for the positive detection of DNA damage.

Terbium(III) (Tb^{3+}) is a trivalent lanthanide cation that possesses low intrinsic fluorescence in aqueous solutions owing to its low absorption cross-section and non-radiative deactivation through the O-H vibrations of the coordinated water molecules [33-40]. Upon chelation of the ion by ligands that, when excited with light, undergo intersystem crossing from the ligand's excited singlet state to an excited triplet state. Following this crossing, radiationless energy transfer occurs from the excited triplet state of the ligand to the lanthanide ion, resulting in population of its excited state. This process leads to longer emission lifetimes with significant fluorescence enhancement, due to the involvement of the long-lived triplet state [33-40]. This property, which allows for efficient intra-molecular energy transfer from ligand to central atom, along with the fact that there is an insignificant degree of radiationless deactivation in the chelated ion [41], has made Tb^{3+} ions extremely valuable as fluorescent probes for detecting DNA [42-45] as well as detecting alkaline metal binding sites in proteins [46,47], tRNA [48], and rRNA [49,50]. Similarly, lanthanides, especially Tb^{3+}, have been employed to study the structure of tRNA [48,51], rRNA [49] and DNA [52,54]. In addition, the enhancement of Tb^{3+} emission in the presence of single-stranded oligonucleotides has been utilized in the detection of distorted DNA regions [55], single base mismatches in DNA duplexes [56] and DNA- and RNA-drug interactions [57,58].

In this paper, we explore the enhanced emission of Tb^{3+} as a potential tool to probe UV-induced DNA damage. This is accomplished by the use of a DNA hairpin probe complementary to the DNA target of interest. The Tb^{3+}/hairpin probe detects UV-induced DNA damage through

the hybridization of the hairpin probe to the undamaged target DNA. The damaged DNA-hairpin hybrid is destabilized, and the probe preferentially acquires the hairpin structure while the damaged target remains single-stranded. The Tb^{3+} then directly coordinates to the unpaired nucleobases of the single-stranded damaged DNA. This enhances the intrinsic fluorescence of Tb^{3+}, producing a detectable signal proportional to the amount of DNA damage. Thus, the recognition of DNA damage is accomplished by the hairpin probes through hybridization reactions and the Tb^{3+} is the reporter that generates a physically measurable signal reflecting the amount of damage. The Tb^{3+}/hairpin probe has superior selectivity and sensitivity for DNA damage compared to conventional DNA MBs, and is almost an order of magnitude less expensive.

2. Experimental

2.1. Materials

Single-stranded oligonucleotide targets and hairpin probes (Scheme 1) were obtained from Integrated DNA Technologies Inc. (Coralville, Iowa). The oligonucleotide samples were purified by standard desalting. The terbium(III) chloride ($TbCl_3$) was obtained from Sigma-Aldrich Canada Ltd. (Oakville, Ontario), magnesium chloride ($MgCl_2$) and sodium chloride (NaCl) were obtained from EMD Chemicals Inc. (Gibbstown, New Jersey), and Tris was obtained from ICN Biomedicals, (Aurora, Ohio). All chemicals were used as received. Nanopure water from a Barnsted Nanopure (Boston, Massachusetts) system was used for all solutions. The oligonucleotide samples were each dissolved in nanopure water and kept frozen at –20 °C until needed.

2.2. Instrumentation

Absorption spectra were recorded at intervals throughout the irradiation period on a Hewlett-Packard (Sunnyvale, California) 8452A diode array spectrophotometer. For the fluorescence measurements were done using a Photon Technologies International (Birmingham, New Jersey) fluorescence spectrophotometer. The change in temperature was monitored by means of a Cole-Parmer DiGi-SENSE thermocouple (Niles, Illinois). Oligonucleotide samples were irradiated in a Luzchem (Ottawa, Ontario) DEV photoreactor chamber with UVC light from lamps emitting principally at 254 nm with an irradiation dose of 75 W m^{-2}.

2.3. Procedures

2.3.1. UV Irradiation

Nitrogen-purged aqueous solutions of 10 μM oligonucleotide targets were irradiated in sealed, UV-transparent 1 cm path length cuvettes. The cuvettes were placed in a water bath in a UV-transparent water dish to keep the temperature constant throughout the irradiation. Oligonucleotide samples were irradiated in the photoreactor chamber with UVC light. The samples were constantly stirred during irradiation, and the photoreactor was purged with nitrogen throughout the irradiation to flush out oxygen and any ozone subsequently generated from the UVC lamps. Control samples were handled identically, but were not exposed to UV radiation. The UVC lamps were turned on ~20 min before the start of irradiation to stabilize the lamp output.

2.3.2. Absorption and fluorescence measurements

Absorption spectra were recorded by placing the irradiated cuvettes containing the target oligonucleotide solutions directly into the spectrophotometer. For the fluorescence

measurements, a 10 μL aliquot of each irradiated solution was taken at various time intervals and was later mixed with appropriate amounts of the hairpin probes and 2 mM Tris buffer solution (pH 7.5) to give final concentrations of 2 μM oligonucleotide targets and 2 μM hairpin probes. These solutions were then incubated in the dark at room temperature for about 24 h. A 40 μM $TbCl_3$ solution was added to the hybridized solutions prior to the fluorescence measurements. For the MB fluorescence measurements, a 10 μL aliquot of each irradiated solution was taken at various time intervals and was later mixed with an appropriate amount of the MB probe and 10 mM Tris buffer solution (3 mM $MgCl_2$, 1 mM EDTA, pH 7.5) to give final concentrations of 1 μM oligonucleotide target and 200 nM MB probe. These solutions were then incubated in the dark at room temperature for about 24 h.

Fluorescence spectra of 100 μL aliquots of the incubated hybridization mixtures were measured. The spectra were recorded between 450 and 600 nm with excitation at 290 nm for the Tb^{3+} fluorescence measurements, and between 500 and 700 nm with excitation at 490 nm for the MB fluorescence measurements. A 1 cm path length Suprasil quartz fluorescence cuvette was used for these measurements.

The Tb^{3+}/hairpin probe was characterized by a thermal denaturation profile experiment, in which temperature-dependent fluorescence measurements were carried out on a buffered 2 μM solution of the hairpin probe incubated in the absence or presence of either the target oligonucleotide sequence or the UV-damaged target sequence at 2 μM concentration. The temperature was varied from 20 to 60 °C in 4 °C increments at a heating rate of 1 °C min^{-1} and 5 min settling time for each step of the heating cycle.

3. **Results and discussion**

156 The hairpin probes used in this study are carefully designed to maximize their performance
157 as a specific probe for UV-induced nucleic acid damage. This design ensures that the probes can
158 selectively discriminate single damage sites in oligonucleotides. Scheme 1 shows the structure of
159 the hairpin probes used in this study. Each probe is composed of a loop and a stem region
160 composed of six base pairs. The design of the hairpin maximizes discrimination of damaged
161 ***versus*** undamaged targets, due to the melting temperatures (T_m's) of the stem and hybrid;
162 designing the hairpin to have a T_m for the stem 5 – 10 °C higher than the T_m of the hybrid
163 ensures maximum selectivity [21].
164 The fluorescence at 545 nm of Tb^{3+} alone, in the presence of single-stranded DNA (ssDNA)
165 and in the presence of double-stranded DNA (dsDNA) is shown in Figure 1. The intrinsic
166 fluorescence of Tb^{3+} is enhanced by ~15 times in the presence of ssDNA, while almost complete
167 fluorescence quenching occurs in the presence of dsDNA (Figure 1). After UV damage, the
168 hairpin probe will hybridize only with the undamaged DNA, while the damaged DNA remains
169 single-stranded, binding Tb^{3+} and enhancing its fluorescence. In this way, the Tb^{3+} produces a
170 detectable signal proportional to the amount of DNA damage. In order to optimize Tb^{3+}/hairpin
171 detection of DNA damage to obtain the maximum discrimination between damaged and
172 undamaged oligonucleotides, we studied the effect of ionic strength, oligonucleotide
173 concentrations, and Tb^{3+} concentration on the fluorescence of Tb^{3+}.
174 *3.1. Optimizing DNA damage detection*
175 The analysis of DNA damage is commonly carried out in the presence of high ionic strength
176 buffers with metal ions such as magnesium and sodium ions present. Such ions are essential for
177 stabilizing the hairpin structure of the probe and the hybrid between the probe and undamaged
178 target [2,21-24]. We studied the effect of magnesium and sodium ions on the enhancement of

179 Tb^{3+} fluorescence in the presence of ssDNA. Figure 2A shows the fluorescence of the Tb^{3+}-
180 ssDNA complex at 545 nm as a function of different concentrations of magnesium and sodium
181 ions that have been previously used in buffers for the detection of DNA damage [2,21-24]. The
182 results show that the highest fluorescence is from solutions of buffers having no Mg^{2+} and Na^{+}.
183 The Tb^{3+} fluorescence decreased with increasing sodium concentrations, with increasing
184 magnesium concentration, and with increasing concentration of both (Figure 2A). These results
185 can be attributed to blocking of Tb^{3+} binding sites on the negatively charged phosphate backbone
186 by the Na^{+} and Mg^{2+} ions, lowering the Tb^{3+} fluorescence. Figure 2A also shows that the
187 presence of Mg^{2+} in the buffer has a more drastic effect on the enhancement of Tb^{3+} fluorescence
188 than Na^{+}, indicating that the higher valance ions lower the enhancement of the Tb^{3+} fluorescence
189 more. To maximize the fluorescence enhancement of Tb^{3+}, 2 mM Tris buffer with no Na^{+} and
190 Mg^{2+} ions added was used for all subsequent measurements.

191 Figure 2B shows a plot of the fluorescence of 25 μM Tb^{3+} as a function of the nucleobase
192 concentration of the single-stranded and double-stranded DNA. In the absence of DNA, Tb^{3+}
193 fluorescence is very low (Figure 2B). Upon addition of the ssDNA, the Tb^{3+} emission increases
194 linearly with increasing ssDNA nucleobase concentration. After the addition of ~29 μM ssDNA
195 bases, the fluorescence enhancement starts to gradually level. This result is expected, as the Tb^{3+}
196 concentration is 25 μM, and indicates that one Tb^{3+} binds, on average, to one base. The annealed
197 duplex solutions did not enhance the Tb^{3+} fluorescence (Figure 2B), as expected, because all the
198 electron donating groups of the nucleoside bases are base-paired and are not free to coordinate to
199 Tb^{3+}. This result confirms that binding to the phosphate backbone, without direct coordination to
200 the base, doesn't result in efficient energy transfer [59,60]. It is worth mentioning that the
201 fluorescence of solutions of both Tb^{3+}- ssDNA and Tb^{3+}-dsDNA complexes did not change over

6 h. This result indicates that the presence of Tb^{3+} with dsDNA does not force the equilibrium to shift to the ssDNA formation over the 6 h period of time and acts only as a multivalent cation stabilizing the hybrid secondary structure.

The fluorescence spectra and intensities of Tb^{3+}-ssDNA complexes strongly depend on the amount of complexed Tb^{3+} (Figure 2C). In the absence of Tb^{3+}, the solution is non-fluorescent as expected. When Tb^{3+} is added to the annealed duplex solutions, no fluorescence enhancement is observed and the fluorescence is constant at the background level. After the addition of Tb^{3+} to the ssDNA solutions, the emission of Tb^{3+} is greatly enhanced, and the fluorescence intensity increases linearly with increasing Tb^{3+} concentration. As shown in Figure 2C, when the Tb^{3+}:nucleobase ratio reaches 1:1, the fluorescence intensity saturates. To ensure complete complexation with ssDNA, a 1.3-fold excess of Tb^{3+} was used in the following experiments to form the Tb^{3+}-ssDNA complexes.

3.2. Selectivity of Tb^{3+}/hairpin detection of DNA damage

To examine the selectivity of this method for the detection of UV-induced DNA damage, we measured the fluorescence at 545 nm of 40 μM Tb^{3+} in the presence of the hairpin probe alone, the annealed duplexes of the hairpin probe with the undamaged target, and with the 5 minute- and 60 minute-UV damaged ssDNA targets for 5 and 60 min as a function of temperature. Figure 3 shows their thermal denaturation profiles. At low temperatures, the fluorescence of Tb^{3+} in the presence of the hairpin probe remains constant at a slightly enhanced fluorescence signal level due to the interaction of Tb^{3+} with the nucleobases in the single-stranded loop of the hairpin probe. At temperatures close to the melting temperature of the stem of hairpin probe (~42 °C), the Tb^{3+} fluorescence gradually increases with temperature, because the proportion of single-stranded DNA increases as the stem melts. For the hybrid between the probe and undamaged

target, there is no fluorescence enhancement at low temperatures, because the undamaged target is completely hybridized with the probe and all the nucleobases are involved in hydrogen bonding. At temperatures close to the hybrid melting temperature (~39 °C), the fluorescence intensity gradually increases due to the interaction of Tb^{3+} with the unpaired nucleobases of the undamaged target.

It is clear that the thermal denaturation profile of the undamaged target-hairpin probe hybrid in the presence of Tb^{3+} shows an opposite trend to that of the MB probe [2,21-24] and this is what causes the Tb^{3+} fluorescence signal to increase with increasing damage to the target. This result is demonstrated in Figure 3, where the hybrid between the hairpin probe and the oligonucleotide target subjected to UVC light for 5 min in the presence of Tb^{3+} shows higher fluorescence intensity than that of the hairpin-undamaged target hybrid and is essentially flat with increasing temperature. The slight decrease in fluorescence with increasing temperature has been observed before [21,22,31] and is attributed to a higher rate of non-radiative relaxation in the fluorophore at higher temperature. The thermal denaturation profile of the hybrid between the hairpin probe and the oligonucleotide target subjected to UV-C light for 60 min in the presence of Tb^{3+} shows a very similar trend to that of the 5 min-irradiated target-hairpin hybrid. This result indicates that most of the oligonucleotide targets are damaged within 5 minutes of UVC irradiation and are in the single-stranded structure causing maximum enhancement of the Tb^{3+} fluorescence. As shown in Figure 3, there is good discrimination in the fluorescence between the undamaged and damaged targets hybridized with the hairpin probe in the presence of Tb^{3+} at 20 °C. Therefore, we have chosen this hybridization temperature for detecting the formation of the UV-induced photoproducts.

In order to confirm that these are the secondary structures of the probe-target hybrids for the undamaged and 5 minute UV-damaged targets, we also measured the 260 nm absorbance of these solutions as a function of temperature (Figure 3 inset). As shown in the inset, the hybrid between the hairpin probe and the UV-damaged target shows a higher absorbance than that of the hybrid between the hairpin and the undamaged target at low temperatures. The increase in absorbance of the damaged solution is due to less hypochromism from the single-stranded damaged target. This confirms that the UV-damaged target-probe hybrid after 5 min is unstable due to damage and the probe preferentially acquires the hairpin structure with the damaged target in the single-stranded form.

To confirm the selectivity of Tb^{3+} to detect single-stranded DNA in the presence of complementary duplexes, we measured the fluorescence intensity as a function of the dsDNA:ssDNA concentration ratio at a total target concentration equal to the Tb^{3+} concentration. Figure 4 shows the resulting calibration curve obtained. At zero ssDNA concentration, i.e. only dsDNA is present in the mixture, Tb^{3+} shows no fluorescence. Upon increasing ssDNA concentration, the Tb^{3+} fluorescence increases linearly. The sensitivity, calculated as the slope of the calibration curve, is 8.21×10^{11}cps M^{-1} and the limit of detection (LOD), calculated as 3 times the standard deviation of the blank divided by the sensitivity, is found to be 28.5 nM. By dividing the concentration of the ssDNA bases by the LOD, we are able to calculate that Tb^{3+} can detect one unpaired nucleobase in the presence of ~10600 paired ones in double-stranded form.

3.3. Detection of UV-induced photoproducts

In order to investigate the selectivity of the Tb^{3+}/hairpin probe to detect nucleic acid damage, T_{random} and $T_{dT_{17}}$ oligonucleotide targets were irradiated separately at constant temperature. The Tb^{3+} fluorescence was measured (Figure 5) after aliquots of both the irradiated and unirradiated samples of these solutions were incubated with the complementary hairpin probes and Tb^{3+}. It should be noted that the hairpin probes were not irradiated, they were only incubated with aliquots of either the irradiated oligonucleotides or unirradiated controls. As shown in Figure 5A and 5B, the Tb^{3+} fluorescence increases with target UV irradiation dose and continues to increase with increasing dose until it reaches a plateau. This plateau is reached within the first 3 min of target irradiation under the conditions used here. No fluorescence is observed from the unirradiated controls. This result indicates that after 3 min irradiation, the entire probe is in the hairpin form and Tb^{3+} exhibits its maximum fluorescence enhancement.

The fluorescence signal as a function of irradiation time for the T_{random} and $T_{dT_{17}}$ oligonucleotide targets (Figure 5A, 5B) were fit to a single exponential growth function. This increase in the fluorescence intensity represents the decreased stability of the damaged target-hairpin hybrid. Therefore, the faster the increase in the fluorescence intensity, the faster the rate of UV-induced damage in the oligonucleotide targets. The damage constants obtained by fitting these fluorescence damage curves are shown in Table 1 for both the T_{random} and $T_{dT_{17}}$ oligonucleotide targets. It is clear from Table 1 that the damage constant of the $T_{dT_{17}}$ target is ~2.8 times faster than that of the T_{random} target. This indicates that the $T_{dT_{17}}$ target is more damaged under UV irradiation than the T_{random} target. Comparing the number of photoreactive damage sites in each target reveals that the $T_{dT_{17}}$ target has 8 TT sites that are most prone to UV damage. However, the T_{random} target has only one TT site, one TC site, three CT sites, one AA site and two AT sites. CPDs are produced preferentially at TT and TC sites, whereas CC and CT

dipyrimidine sites are poorly photoreactive [13], and dipurine sites are photostable compared to dipyrimidine sites [1]. So the T_{random} target contains a total of five dipyrimidine sites, in which four of them are less photoreactive than the TT site. Thus, it should exhibit slower photodamage kinetics, consistent with Figure 5. This result confirms that we can get information on the amount of UV damage accumulated in different targets by comparing the damage constant values obtained by the same probe.

The selectivity of the Tb^{3+}/hairpin probe was compared to the MB for detecting nucleic acid damage. The MB probe (Scheme 1) used in this study was designed to have the same sequence as the hairpin probe, i.e. complementary to the T_{dT17} target. In this target, the 260 nm absorption band bleaches with increasing irradiation time, quantifying photoproduct formation via the loss of the C_5=C_6 and yielding an independent spectroscopic marker for DNA damage.

As explained above, the MB fluorescence is quenched in the hairpin position when the FAM fluorophore and DABCYL quencher are in close proximity, and the fluorescence intensity is high in the presence of complementary target when the MB forms a hybrid with the target. As damage accumulates on the target strand, the MB-target hybrid becomes less stable, effectively decreasing the fluorescence intensity until the closed, hairpin form is the more stable form of the MB. This trend is shown in Figure 5C, in which the MB fluorescence intensity decreases with longer target irradiation time until reaching a constant minimum corresponding to the quenched fluorescence of the MB in the hairpin structure. The damage curve for MB-detected UV damage was fit to a single exponential decay function. The damage constant obtained is shown in Table 1. The selectivity of the probe is directly related to the damage constant; the faster the fluorescence intensity increases in case of Tb^{3+}/hairpin probe (Figure 5B) or decreases in case of

313 the MB probe (Figure 5B), the more selective the probe is at detecting UV-induced DNA
314 damage under identical irradiation conditions for the same target. Table 1 shows that the damage
315 constant of the Tb^{3+}/hairpin probe is 6 times faster than that of the DNA MB. This proves that
316 the Tb^{3+}/hairpin probe has superior selectivity for detection of UV damage in nucleic acids
317 compared to the DNA MB method.

318 UV absorbance measurements as a function of $T_{dT_{17}}$ target irradiation time (Figure 5D) were
319 used to quantify the amount of UV damage and to develop calibration curves for the Tb^{3+}/hairpin
320 probe. This curve was fit to a double-exponential function and the damage constants are listed in
321 Table 1. The results show that the damage constant of the Tb^{3+}/hairpin probe is 15 times faster
322 than the fastest absorption damage constant. This confirms that the fluorescent Tb^{3+}/hairpin
323 probe has superior selectivity for detection of UV damage in nucleic acids over the absorption
324 method [2,22,31].

325 *3.4. Sensitivity of the Tb^{3+}/hairpin probe*

326 In order to check the sensitivity of the Tb^{3+}/hairpin probe for damage detection, we used the
327 UV absorbance measurements as a function of target irradiation time to quantify the amount of
328 UV damage and to develop calibration curves of the UV-induced photoproducts detected by the
329 Tb^{3+}/hairpin probe. The procedure and calculation of the photoproducts concentration from the
330 absorbance measurements of the irradiated solutions have been explained previously [31]. Figure
331 6 shows the calibration curve obtained upon plotting the Tb^{3+} fluorescence intensity as a function
332 of the concentration of the photoproducts calculated for both the Tb^{3+}/hairpin probe (Figure6A)
333 and the fluorescence signal for the MB probes (Figure 6B). In Figure 6A, the fluorescence at
334 zero concentration of the photoproducts represents the background level corresponding to the

quenched Tb^{3+} fluorescence as the hairpin probe is completely hybridized with the undamaged target. The Tb^{3+} fluorescence increases linearly with increasing damage. At high damage concentrations, the hybrids formed between the hairpin probe and the damaged strands are completely unstable, and the probe acquires the hairpin structure with the damaged target in the single-stranded form leading to maximum enhancement of Tb^{3+} fluorescence. Additional formation of photoproducts cannot lead to any more dehybridization, so the fluorescence signal shows saturation-like behaviour.

For the DNA MB (Figure 6B), any decrease in fluorescence signal requires a minimum 2.59 μM concentration of the photoproducts. The constant fluorescence signal of the DNA MB over the range of 0 – 2.59 μM of the photoproducts concentration can be attributed to the lower selectivity of the DNA MB to UV-induced DNA damage as discussed above. At high photoproduct concentrations, the hybrid formed between the DNA MB and the damaged strand is completely unstable, and the DNA MB preferentially acquires the hairpin structure where the fluorophore and the quencher are in close proximity and the fluorescence is the lowest. Further damage doesn't lead to any additional decrease in fluorescence and the signal remains constant, showing a saturation-like behaviour.

Although the MB probe used in this study was designed to have the same sequence as the hairpin probe (Scheme 1), the Tb^{3+}/hairpin probe proved to be more selective and sensitive to UV-induced DNA damage than the MB probe. This can be attributed to the difference in the reporting mechanism between the two probes. In the MB probe, the reporting mechanism is through FRET between a fluorophore-quencher pair on the hairpin probe, while in the Tb^{3+}/hairpin probe, it is through direct emission from the coordinated Tb^{3+} via energy transfer from the unpaired nucleobases. This is reflected in Figure 6A where the low fluorescence

358 background allowed the Tb^{3+} to show an immediate fluorescence increase upon photoproduct
359 formation, leading to better sensitivity. Also, it has been previously shown that single
360 mismatches in the sequence of a duplex DNA lead to selective Tb^{3+} fluorescence enhancement
361 [56]. Our result showing that Tb^{3+} is sensitive to very low photoproduct concentrations is
362 consistent with this past work. For the MB probe (Figure 6B), the high fluorescence background
363 of the quenched fluorophore decreases the sensitivity of this probe.
364 Table 2 shows the parameters for the quantification of UV-induced DNA damage from Figure 6.
365 The calibration curve for the Tb^{3+}/hairpin probe shows a similar linear dynamic range to the MB
366 probe (Table 2), taking into account the MB threshold response of 2.59 μM photoproduct. The
367 sensitivity of detection is larger by a factor of ~2.5 for the Tb^{3+}/hairpin probe, leading to a lower
368 limit of detection (LOD) and limit of quantification (LOQ) by approximately an order of
369 magnitude. It is worth mentioning that the values recorded in Table 2 for the LOD and LOQ for
370 the MB method for the detection of DNA damage is obtained by using the standard deviation of
371 the blank measurements and the sensitivity of the method, while the LOD and LOQ will be
372 practically limited to the threshold 2.59 μM (Figure 6B) photoproduct concentration. From this
373 data, we calculate that the Tb^{3+}/hairpin probe can detect one damage site in the presence of
374 ~8000 undamaged sites, compared to one damage site in the presence of ~820 undamaged sites
375 with the MB probe. This again confirms the superior sensitivity of the Tb^{3+}/hairpin probe over
376 the MB probe. Considering the volume of the DNA target solution used in one analysis (100
377 μL), our technique allows the detection of 0.4 picomoles of UV-damaged sites. The detection
378 limit of this technique compares favorably with those reported for other DNA damage
379 techniques, such as mass spectrometry [12], alkaline gel electrophoresis [61], immunoassay
380 coupled with laser-induced fluorescence [17], ELISA [62], electrochemical detection [10] and

HPLC-MS/MS [63]. This detection limit allows the Tb^{3+}/hairpin probe to be used in high-throughput, quantitative analysis of DNA damage.

Conclusions

These results conclusively show that the Tb^{3+}/hairpin probe is a sensitive tool for detecting UVC-induced oligonucleotide damage. Changing the fluorescence reporting mechanism of the probe from a fluorophore-quencher pair attached to the hairpin probe to Tb^{3+} coordinated to ssDNA allows positive detection of DNA damage with a fluorescence signal that increases with increasing damage. The Tb^{3+}/hairpin probe proves to have superior selectivity and sensitivity to DNA damage than the MB probe, while also being much cheaper and easier to synthesize. The Tb^{3+}/hairpin probe represents a promising tool in the design of biosensors for the *in vivo* detection of the nucleic acid damage. The only limitation of this technique is that a specific probe sequence must be designed for each DNA target. Upon comparing this requirement to the complexity of other available and widely used techniques for the detection of DNA damage, such as HPLC-MS/MS and fluorescently labelled antibodies, the Tb^{3+}/hairpin probe method is still cheaper and simpler.

4. Acknowledgements

The authors acknowledge financial support for this work from the Canadian Natural Sciences and Engineering Research Council (NSERC) Discovery Grants-in-aid.

5. References

[1] B. P. Ruzsicska, D. G. E. Lemaire, in: W. M. Horspool, P.-S. Song, (Eds.), DNA Photochemistry, CRC Handbook of Organic Photochemistry and Photobiology; CRC Press, New York. 1995, pp. 1289-1317.

[2] S. Yarasi, C. McConachie, G. R. Loppnow, Photochem. Photobiol. 81 (2005) 467-473.

[3] B. Ames, L. Gold, W. Willett, Proc. Natl. Acad. Sci. U.S.A. 92 (1995) 5258-5265.

[4] T. Lindahl, Nature. 362 (1993) 709-715.

[5] L. Marnett, P. Burcham, Chem. Res. Toxicol. 6 (1993) 771-785.

[6] L. Marrot, J. Meunier, J. Am. Acad. Dermatol. 58 (2008) S139-S148.

[7] M. Weinfeld, K. Soderlind, Biochemistry (N.Y.) 30 (1991) 1091-1097.

[8] X. Le, J. Xing, J. Lee, S. Leadon, M. Weinfeld, Science. 280 (1998) 1066-1069.

[9] B. Haab, R. Mathies, Anal. Chem. 67 (1995) 3253-3260.

[10] K.C. Kucharikova, M. Fojta, T. Mozga, E. Palecek, Anal. Chem. 77 (2005) 2920-2927.

[11] H. Kaur, B. Halliwell, Biochem. J. 318 (1996) 21-23.

[12] I. D. Podmore, M.S. Cooke, K.E. Herbert, J. Lunec, Photochem. Photobiol. 64 (1996) 310-315.

[13] T. Douki, J. Cadet, Biochemistry (N.Y.) 40 (2001) 2495-2501.

[14] J. Ravanat, T. Douki, J. Cadet, Photochem. Photobiol. B Biol. 63 (2001) 88-102.

[15] A. Kumar, M. Tyagi, P. Jha, Biochem. Biophys. Res. Commun. 318 (2004) 1025-1030.

[16] C.C. Trevithick-Sutton, L. Mikelsons, V. Filippenko, J. C. Scaiano, Photochem. Photobiol. 83 (2007) 556-562.

[17] J. Xing, J. Lee, S. Leadon, M. Weinfeld, X. Le, Methods 22 (2000) 157-163.

[18] S. Tyagi, D. Bratu, F. Kramer, Nat. Biotechnol. 16 (1998) 49-53.

425 [19] S. Tyagi, F. Kramer, Nat. Biotechnol. 14 (1996) 303-308.
426 [20] K. Wang, Z. Tang, C. J. Yang, Y. Kim, X. Fang, W. Li, Y. Wu, C. D. Medley, Z. Cao, J.
427 Li, P. Colon, H. Lin, W. Tan, Angew. Chem. Int. Ed. Engl. 48 (2009) 856-870.
428 [21] A. F. El-Yazbi, G. R. Loppnow, Can. J. Chem. 89 (2011) 402-408.
429 [22] S. A. Oladepo, G. R. Loppnow, Anal. Bioanal. chem. 397 (2010) 2949-2957.
430 [23] Z.J. Shire, G. R. Loppnow, Photochem. Photobiol. 88 (2012) 645-650.
431 [24] Z.J. Shire, G. R. Loppnow, Anal. Bioanal. chem. 403 (2012) 179-184.
432 [25] K. Stohr, B. Hafner, O. Nolte, J. Wolfrum, M. Sauer, D. Herten, Anal. Chem. 77 (2005)
433 7195-7203.
434 [26] J. Knemeyer, N. Marme, M. Sauer, Anal. Chem. 72 (2000) 3717-3724.
435 [27] A. Misra, P. Kumar, K.C. Gupta, Anal. Biochem. 364 (2007) 86-88.
436 [28] T. Heinlein, J. Knemeyer, O. Piestert, M. Sauer, J. Phys. Chem. B 107 (2003) 7957-7964.
437 [29] Y. Kim, C. J. Yang, W. Tan, Nucl. Acids Res. 35 (2007) 7279-7287.
438 [30] A. Misra, M. Shahid, Bioorg. Med. Chem. 17 (2009) 5826-5833.
439 [31] A. F. El-Yazbi, G. R. Loppnow, Anal. Chim. Acta. 726 (2012) 44-49.
440 [32] A. F. El-Yazbi, G. R. Loppnow, Can. J. Chem. (2013) In press
441 [33] N. Sabbatini, M. Guardigli, J. Lehn, Coord. Chem. Rev. 123 (1993) 201-228.
442 [34] S. Rigault, C. Piguet, G. Bernardinelli, G. Hopfgartner, Angew. Chem. Int. Ed. 37 (1998)
443 169-172.
444 [35] N. Martin, J. Bunzli, V. McKee, C. Piguet, G. Hopfgartner, Inorg. Chem. 37 (1998) 577-
445 589.
446 [36] C. Piguet, J. Bunzli, G. Bernardinelli, G.Hopfgartner, S.Petoud, O. Schaad, J. Am.
447 Chem. Soc. 118 (1996) 6681-6697.

[37] V. Alexander, Chem. Rev. 95 (1995) 273-342.

[38] G. Choppin, Z. Wang, Inorg. Chem. 36 (1997) 249-252.

[39] P. Valente, S. Lincoln, K. Wainwright, Inorg. Chem. 37 (1998) 2846-2847.

[40] M. Wolbers, F. van Veggel, B. SnellinkRuel, J. Hofstraat, F. Geurts, D. Reinhoudt, J. Am. Chem. Soc. 119 (1997) 138-144.

[41] R. C. Leif, L. M. Vallarino, M.C. Becker, S. Yang, Cytometry A 69A (2006) 767-778.

[42] M. Li, P. R. Selvin, Bioconjug. Chem. 8 (1997) 127-132.

[43] A. Saha, K. Kross, E. Kloszewski, D. Upson, J. Toner, R. Snow, C. Black, V. Desai, J. Am. Chem. Soc. 115 (1993) 11032-11033.

[44] P. Ioannou, T. Christopoulos, Anal. Chem. 70 (1998) 698-702.

[45] P. Hurskainen, P. Dahlen, J. Ylikoski, M. Kwiatkowski, H. Siitari, T. Lovgren, Nucl. Acids Res. 19 (1991) 1057-1061.

[46] S. Ghosh, A. Misra, A. Ozarowski, A. Maki, J. Phys. Chem. B. 107 (2003) 11520-11526.

[47] A. Leonov, B. Voigt, F. Rodriguez-Castaneda, P. Sakhaii, C. Griesinger, Chem. Eur. J. 11 (2005) 3342-3348.

[48] M. J. Belousoff, P. Ung, C. M. Forsyth, Y. Tor, L. Spiccia, B. Graham, J. Am. Chem. Soc. 131 (2009) 1106-1114.

[49] M. Lambert, J. Hoerter, M. Pereira, N. Walter, RNA 11 (2005) 1688-1700.

[50] A. Trentani, P. Testillano, M. Risueno, M. Biggiogera, Eur. J. Histochem. 47 (2003) 195-200.

[51] M. Roy, L. Wittenhagen, S. Kelley, RNA 11 (2005) 254-260.

[52] B. Jolles, A. Laigle, J. Liquier, L. Chinsky, Biophys. Chem. 46 (1993) 179-185.

[53] S. Klakamp, W. Horrocks, J. Inorg. Biochem. 46 (1992) 175-192.

[54] D. Gersanovski, P. Colson, C. Houssier, E. Fredericq, Biochim. Biophys. Acta. 824 (1985) 313-323.

[55] Z. Balcarova, V. Brabec, Biophys. Chem. 33 (1989) 55-61.

[56] P. Fu, C. Turro, J. Am. Chem. Soc. 121 (1999) 1-7.

[57] L. Pearlman, H. Simpkins, Biochem. Biophys. Res. Commun. 131 (1985) 1033-1040.

[58] Y. Ci, Y. Li, X. Liu, Anal. Chem. 67 (1995) 1785-1788.

[59] A. Canfi, M. Bailey, B. Rocks, Analyst. 114 (1989) 1405-1406.

[60] A. Abusaleh, C. Meares, Photochem. Photobiol. 39 (1984) 763-769.

[61] S.E. Freeman, A.D. Blackett, D.C. Monteleone, R.B. Setlow, B.M. Sutherland, J.C. Sutherland, Anal. Biochem. 158 (1986) 119-129.

[62] M.S. Cooke, I.D. Podmore, N. Mistry, M.D. Evans, K.E. Herbert, H.R. Griffiths, J. Lunec, J. Immunol. Methods 280 (2003) 125-133.

[63] F. Zhang, W.T. Scott, A.J. Clark, M.R. Schisler, J.J. Grundy, B.B. Gollapudi, M.J. Bartels, Rapid Commun. Mass Spectrom. 21 (2007) 3949-3955.

6. Figure captions

Scheme1. Sequences of the probes used in this work. The Tb^{3+}/hairpin probes are complementary to T_{random} (A) and to $T_{dT_{17}}$ (B). The MB probe is complementary to $T_{dT_{17}}$ (C). "FAM" denotes the 6-carboxyfluorescein fluorophore and "DABCYL" denotes the dabcyl quencher. T_{random} and $T_{dT_{17}}$ are the oligonucleotide targets used in this study.

Figure 1. The fluorescence spectra of Tb^{3+} alone (—), in the presence of single-stranded DNA (------) and in the presence of double-stranded DNA(·-·-·-). The fluorescence excitation wavelength was 290 nm and the spectra were recorded at room temperature. "c.p.s." denotes counts per second.

Figure 2. Tb^{3+} fluorescence intensity as a function of (A) sodium and magnesium ion concentrations in 2 mM Tris (pH 7.5) buffer and 25 μM Tb^{3+}, (B) nucleobase concentration of single-stranded DNA (open squares) and double-stranded DNA (filled squares) in 2 mM Tris buffer (pH 7.5) and 25 μM Tb^{3+}, and (C) Tb^{3+} concentration of single-stranded DNA (open squares) and double-stranded DNA (filled squares) in 2 mM Tris buffer (pH 7.5) and 34 μM nucleobases. Fluorescence excitation and emission wavelengths were 290 and 454 nm, respectively. Each data point is an average of three replicate measurements and the error bars correspond to the standard deviation of each measurement. "c.p.s." denotes counts per second.

Figure 3. Fluorescence thermal denaturation profiles for 40 μM Tb^{3+}/hairpin probe alone (open circles), 40 μM Tb^{3+}/hairpin probe in the presence of an equimolar amount of the complementary oligonucleotide target sequence (filled circles), and 40 μM Tb^{3+}/hairpin probe in the presence of

513 an equimolar amount of the UV-irradiated oligonucleotide target sequence for 5 min (filled
514 squares) and 60 min (filled triangles). The inset shows the absorption thermal denaturation
515 curves for the same solutions of 40 μM Tb^{3+}/hairpin probe in the presence the complementary
516 oligonucleotide target (filled circles), and the 5 min UV-irradiated oligonucleotide target (filled
517 squares) in 1 cm cuvettes. The lines are guides for the eye.

518 **Figure 4.** Calibration curve of the detection of ssDNA in a mixture of single-stranded and
519 double-stranded DNA with 40 μM Tb^{3+}. [dsDNA] and [ssDNA] are in μM. Each data point is an
520 average of three replicate measurements and the error bars correspond to the standard deviation
521 of the measurements. The linear regression coefficient squared, R^2, calculated from the
522 calibration curve is 0.993, the sensitivity, calculated as the slope of the calibration curve, is 8.21
523 x 10^{11} cps M^{-1}, the limit of detection (LOD), calculated as 3 times the standard deviation of the
524 blank divided by the sensitivity, is found to be 28.5 nM, and the limit of quantification (LOQ),
525 calculated as 3.3 times the LOD, is equal to 95.1 nM. For the determination of the blank standard
526 deviation, 20 solutions of 40 μM Tb^{3+} were measured and the standard deviations of these
527 measurements were 0.7×10^4.

528 **Figure 5**. UV damage plots of Tb^{3+}/hairpin probe fluorescence intensity (λ_{ex} = 290 nm, λ_{em} =
529 545 nm) as a function of target irradiation time for T_{random} (A) and $T_{dT_{17}}$ (B). (C) MB hairpin
530 probe fluorescence (λ_{ex} = 490 nm, λ_{em} = 520 nm) as a function of target irradiation time for $T_{dT_{17}}$.
531 (D) 260 nm absorbance as a function of target irradiation time for $T_{dT_{17}}$. For all experiments, the
532 2 μM irradiated oligonucleotide targets (open squares) and the 2 μM unirradiated control (filled
533 squares) were hybridized with the probe at 20 °C. The solid line through the irradiated sample
534 fluorescence points in (A) and (B) is a single exponential growth fit to $I_F = I_{F,0} + a\,(1 - e^{-t/\tau})$,

where (A) $I_{F,0} = (0.10 \pm 0.01) \cdot 10^5$ cps, a = 4.6 ± 0.01, and $\tau = 1.1 \pm 0.02$ min, and (B) $I_{F,0} = (0.17 \pm 0.01) \cdot 10^5$ cps, a = 3.7 ± 0.01, and $\tau = 0.40 \pm 0.01$ min. The MB damage curve in (C) is a single exponential decay fit to $I_F = I_{F,0} + a\, e^{-t/\tau}$ where $I_{F,0} = (1.2 \pm 0.04) \cdot 10^5$ cps, a = 2.5 ±0.10, and $\tau = 2.36 \pm 0.10$ min. The solid line through the absorbance points (open squares) is the least-squares fit to an offset, double exponential function, $A = A_0 + A_1 e^{t/\tau 1} + A_2 e^{t/\tau 2}$, where the absorbance damage constants are 6.1 ± 0.07 min (τ_1) and 91.8 ± 2.0 min (τ_2), and the amplitudes are $A_1 = 0.52 \pm 0.01$ and $A_2 = 0.66 \pm 0.02$. The offset (A_o) is 0.21 ± 0.02. The control points (filled squares) are fit to a straight line with zero slope by eye.

Figure 6. Calibration curve of DNA photodamage formed upon UV irradiation of the $T_{dT_{17}}$ target for the (A) Tb^{3+}/hairpin probe and (B) DNA MB. The inset shows the fit to the linear portions of the calibration curves. Each data point is an average of three replicate measurements and the error bars correspond to the standard deviation of the measurements.

555

556 **Table 1. Damage constants of the different DNA damage assay methods.**

Method	Damage constant (min)[a]
Tb^{3+}/hairpin probe fluorescence	$\tau_{dT_{17}} = 0.40 \pm 0.01$ $\tau_{random} = 1.10 \pm 0.02$
DNA MB fluorescence	$\tau_{dT_{17}} = 2.36 \pm 0.20$
Absorbance	$\tau_1 = 6.1 \pm 0.07$ $\tau_2 = 92 \pm 2.00$

557 [a]The damage constants (τ) were obtained from the exponential fits in Figure 5.

558

559

560

561

562

563

564

565

566

567

Table 2. Analytical parameters for the quantification of UV-induced DNA damage with Tb^{3+}/hairpin probe and DNA MB

Parameter[a]	Detection of UV-damaged DNA	
	Tb^{3+}/hairpin probe	**DNA MB**
Linear Dynamic Range (μM)	0.00 – 1.72	2.59 – 4.53
R^2	0.975	0.995
Sensitivity (cps M^{-1})	2.38×10^{12}	9.84×10^{11}
LOD (nM)	4.36	41.4
LOQ (nM)	14.5	138

For the determination of the blank standard deviation, 20 solutions of 40 μM Tb^{3+} and 200 nM DNA MB were used, respectively. The standard deviations of these measurements were 0.7×10^4 and 1.3×10^4 c.p.s., respectively. [a]In this table, linear dynamic range is the concentration range corresponding to the linear region in the calibration curve, R^2 is the linear regression coefficient squared, sensitivity is the slope of the calibration curve, LOD is the limit of detection and is 3 times the standard deviation of the blank divided by the sensitivity, and LOQ is the limit of quantification and is 3.3 times the LOD.

585

586 Scheme 1

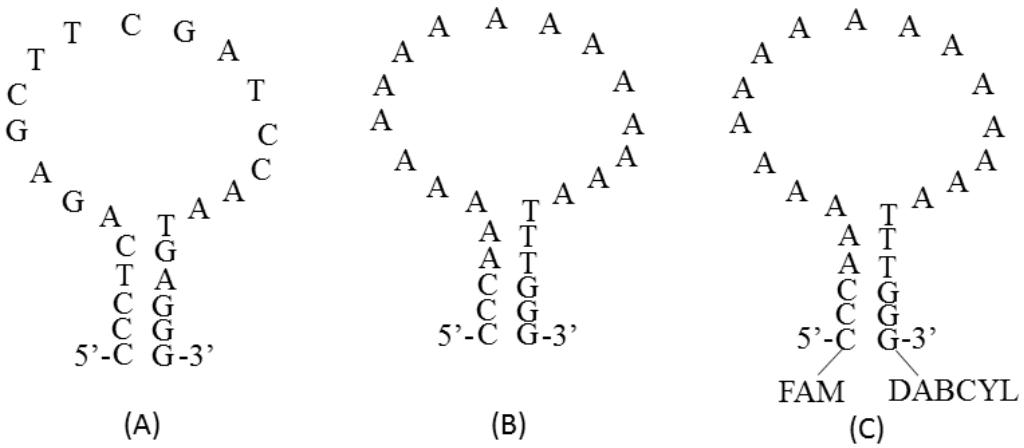

T_{dT17}: 3'-TTT TTT TTT TTT TTT TT-5'

T_{random}: 3'-CTC GAA GCT AGG TTA CT-5'

587

588

589

590

591

592

593

594

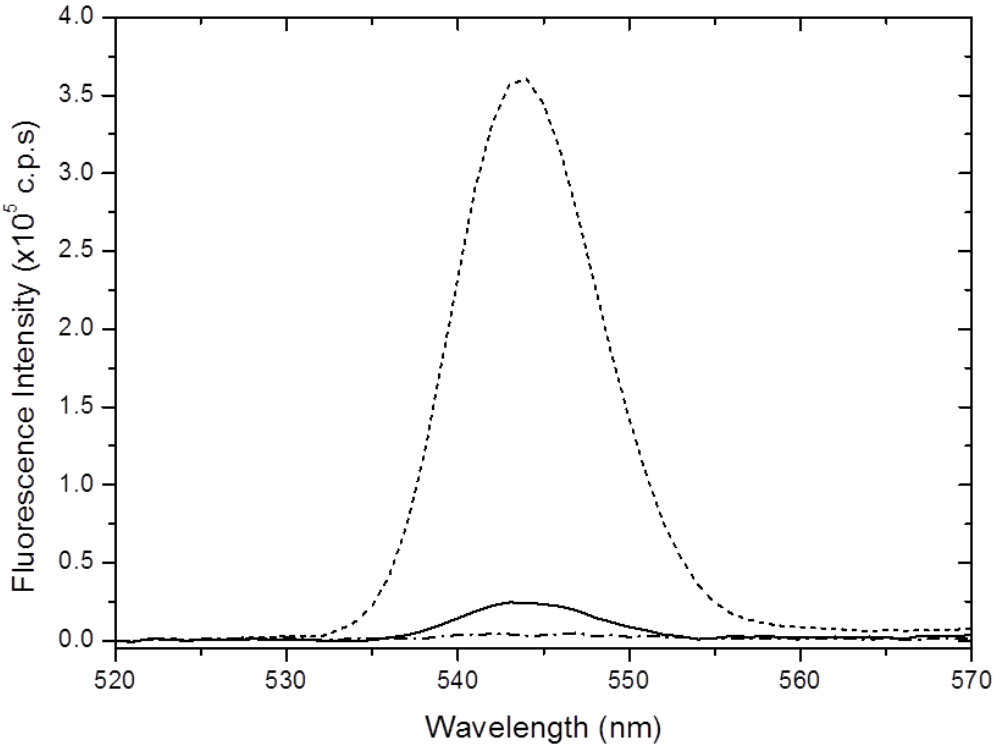

595

596 Figure 1

597

598

599

600

601

602

603

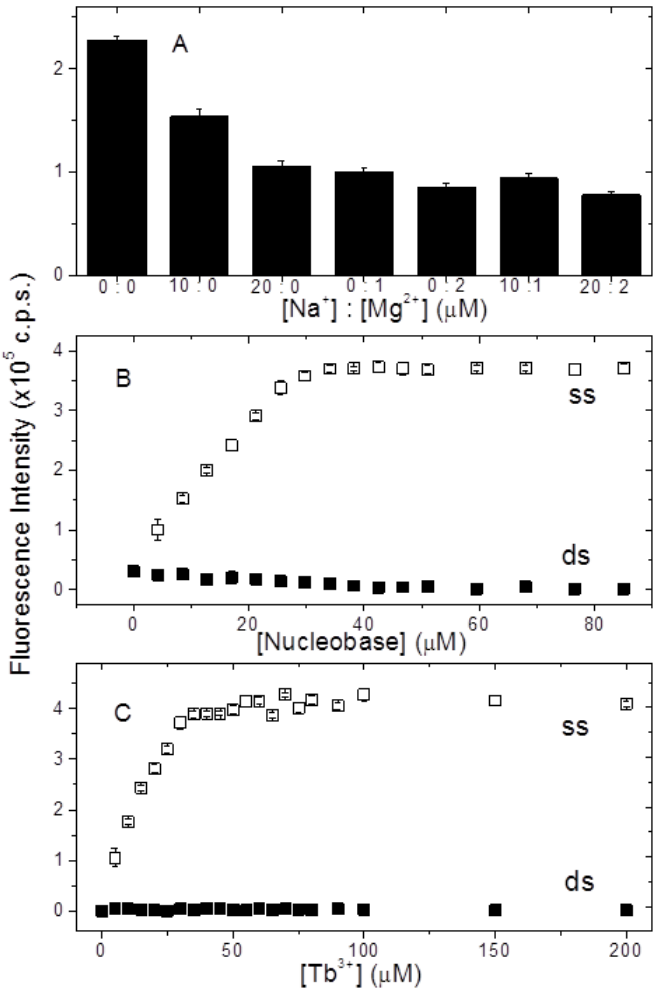
A
0 : 0
10 : 0
20 : 0
0 : 1
0 : 2
10 : 1
20 : 2
[Na+] : [Mg2+] (μM)
B
ss
ds
[Nucleobase] (μM)
C
ss
ds
[Tb3+] (μM)
Fluorescence Intensity (x10^5 c.p.s.)

Figure 2

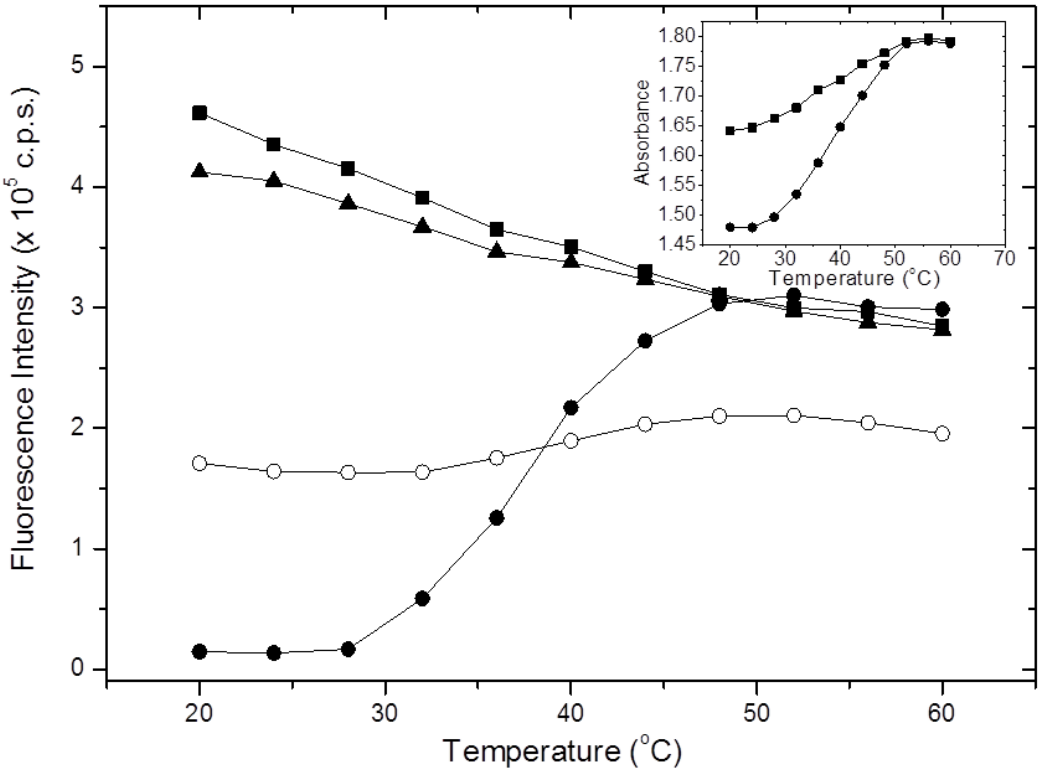

609

610 Figure 3

611

612

613

614

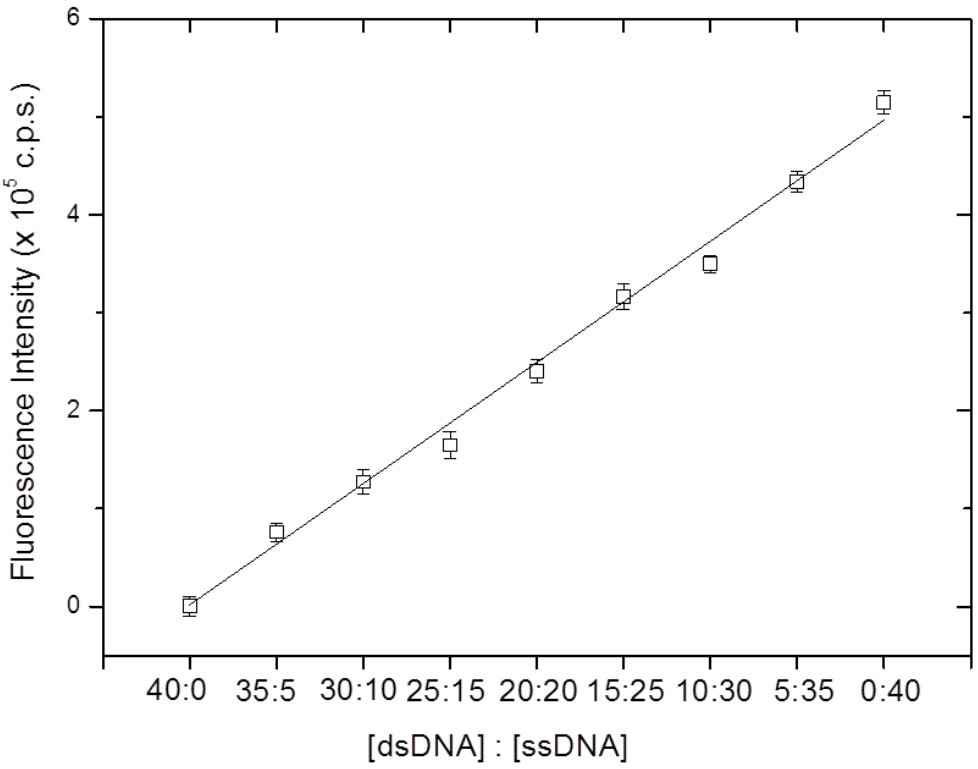

615

616 Figure 4

617

618

619

620

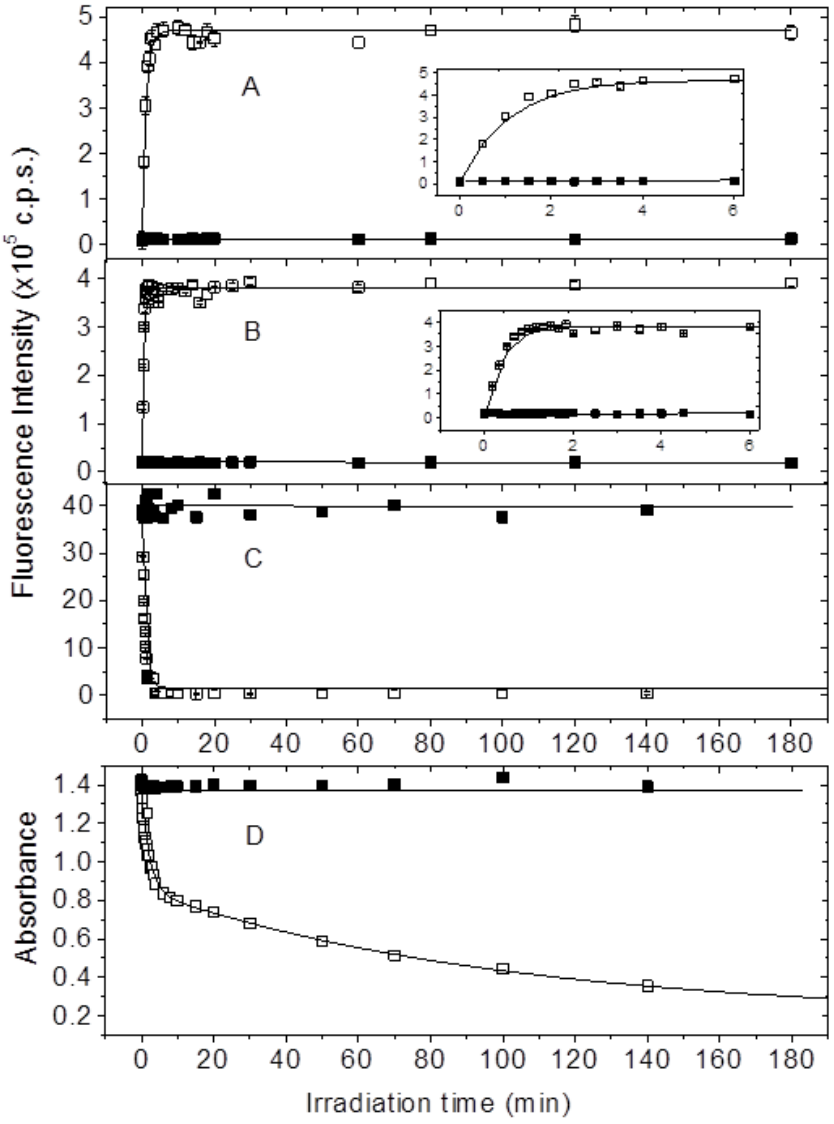

621
622

623 Figure 5

624

625

626

627

628

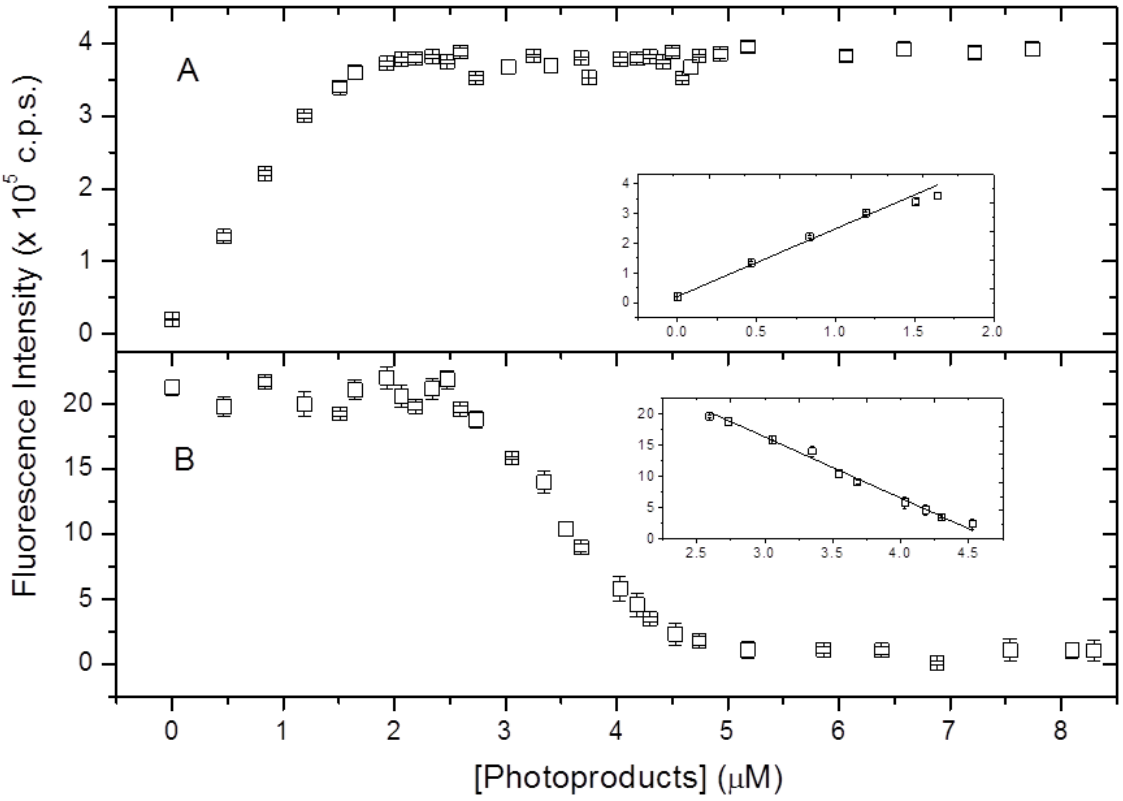

629

630

631

632 Figure 6

633